A molecular beam investigation of He, CO, and O_2 scattering from Pd(111)

Cite as: J. Chem. Phys. **69**, 373 (1978); https://doi.org/10.1063/1.436363
Published Online: 11 August 2008

T. Engel

A molecular beam investigation of He, CO, and O_2 scattering from Pd(111)

T. Engel[a)]

Institut für Physikalische Chemie, Universität München, Sophienstrasse 11, D-8000 München 2, West Germany
(Received 22 February 1978)

Adsorption of CO and O_2 on Pd(111) has been studied with the molecular beam technique. Absolute sticking coefficients for CO and O_2 have been determined as a function of coverage, angle of incidence, and substrate temperature. Angular distributions of the scattered molecules show that the probability for capture in the precursor state is unity for CO at low coverages and for all substrate temperatures investigated and 0.5 for O_2 at low coverages independent of the substrate temperature. Modulated beam experiments show that $E_{des.}$ for CO is 32 kcal/mole at low coverages. Phase sensitive detection and waveform analysis show that at high CO coverages on the impurity free surface and over a wide range of coverages on a carbon contaminated surface, three distinct CO species are present on the surface.

I. INTRODUCTION

Molecular beam techniques applied to surfaces[1-5] have yielded a better understanding of the elementary steps involved in the overall scattering process. Most of the attention to date has been focussed on He and H_2 scattering under conditions for which the surface residence time is extremely small. For chemisorption systems, some measurements of absolute sticking coefficients[6-8] and their angular dependence[6,9], angular distributions for scattered molecules[10,11] and activation energy for desorption[12-14] have been reported. However, the investigations to date are small in number and often only one of the above mentioned system parameters have been determined without attempting to gain a better understanding of the mechanism of the adsorption–desorption process. In this study the chemisorption of both CO and O_2 on a Pd(111) surface has been investigated more fully prior to a study of the CO oxidation reaction.[15] Previous studies of the chemisorption of CO and O_2 on Pd (111) have shown that CO is molecularly absorbed with a high initial sticking coefficient and that a series of ordered structures depending on coverage are formed.[16] The isosteric heat of adsorption is 34 kcal/mole up to $\theta = 1/3$.[17] A saturation coverage of $\theta = 0.66$ is reached at 200 K. O_2 is dissociatively adsorbed,[18] leading at 300 K to the formation of a $p(2 \times 2)$ structure corresponding to $\theta = 0.25$. Adsorption at temperatures greater than 1000 K leads to incorporation of oxygen into the bulk which cannot be removed thermally.[16]

II. EXPERIMENTAL

The apparatus used in this study consisted of two separate subsystems which are shown in Figs. 1 and 2. Figure 1 shows a schematic drawing of the bakable stainless steel beam generating system whose principal parts are nozzle, skimmer, collimating apertures, and three diffusion pump stages, each of which has a pumping speed of 500 l/sec above the gate valve and the liquid nitrogen cooled baffle. The first and second stages handle nearly all of the gas load whereas the third stage serves as a buffer between the high vacuum in the collimator stage and the UHV system. During operation typical pressures in the individual stages were as follows: nozzle chamber 300 torr, nozzle–skimmer chamber 8×10^{-4} torr, collimation stage 4×10^{-6} torr, and buffer stage 3×10^{-8} torr. The last collimation aperture could be varied in operation, permitting five beam widths between 6 and 1 mm at the scattering center. The intensity profile of the beam was nearly trapezoidal in shape with the region of constant intensity approximately 60% of the half width.

The beam system was separated by a straight-through valve from the stainless steel UHV system shown schematically in Fig. 2. The single crystal target is mounted on the system axis which is also the rotation axis of the quadrupole mass spectrometer. By rotating the quadrupole, angular distributions of backscattered particles in the scattering plane can be measured. The distance between the ion source of the quadrupole and the scattering center could be varied under operating conditions and was normally 50 mm. The angular resolution was determined by the beam diameter and divergence at the surface since only one collimating aperture was placed between the surface and the ion source. As the angular divergence of the beam was only 0.02° for a 1 mm beam and 0.1° for a 5 mm beam, the resolution was determined by the beam diameter. For He scattering, for which a high resolution was required, a beam diameter of 1 mm corresponding to 1° resolution was used, whereas for diffuse scattering a 5 mm beam was used which led to a higher signal at the detector and an angular resolution of 5°. The pumping speed of the system for O_2 and CO was increased by evaporating a titanium film in the UHV system at the height of the scattering plane. During operation with a beam intensity equivalent to 4×10^{-7} torr with a half-width of 6 mm the background pressure at the detector always remained below 1×10^{-10} torr. The surface structure and composition could be examined with a LEED–Auger analyzer and an ion gun was available for cleaning cycles. The LEED optics was mounted on a bellows and was completely retracted from the system

[a)] Present address: IBM Research Laboratory Zürich, CH-8803 Rüschlikon, Switzerland.

 0021-9606/78/6901-0373$01.00

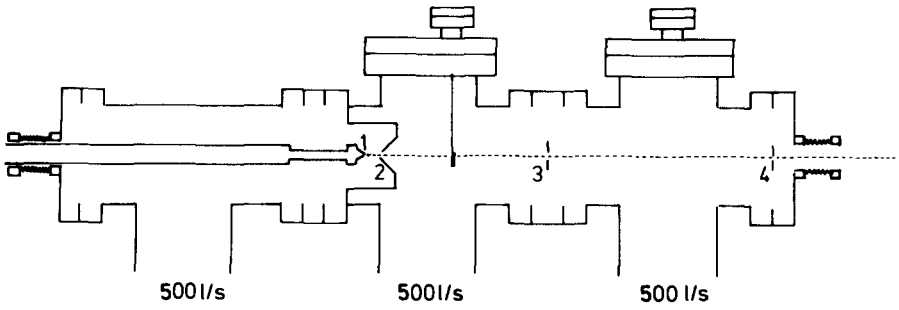

FIG. 1. Schematic diagram of the beam generating apparatus: 1, nozzle; 2, skimmer; 3,4, collimating apertures. Each stage is pumped with liquid nitrogen baffled oil diffusion pumps.

when not in use, so that spurious scattering in the vicinity of the target was minimized. The beam could be modulated by a four bladed chopper driven by an external motor through a magnetic coupling. A reference signal for phase sensitive detection of the scattered intensity was obtained using the light pipe shown in Fig. 2.

The Pd (111) surface was prepared by spark erosion, and mechanical polishing with diamond paste down to 3μ before electropolishing.[19]

III. RESULTS

A. He scattering from Pd(111)

As has been shown previously,[20,21] He is scattered predominantly quasielastically from a well prepared clean, monocrystalline metal surface. For close packed planes only a small contribution from diffracted beams other than the (00) beam is seen.[22,23] It has also been pointed out[24] that the intensity of the specular beam is a sensitive measure of surface smoothness and that it provides valuable information additional to LEED and AES in assessing the degree of order of a clean metal surface. In particular, angular distributions of gas molecules scattered from a surface are not very meaningful unless it can be shown that He scattered from the same surface gives rise to a highly specular pattern.

He scattered from Pd(111) follows the trends previously reported for other metal surfaces.[25] The specular intensity increases with the angle of incidence (measured from the surface normal). The angular width of the scattered beam increases with decreasing angle of incidence. Moreover, the intensity of the specular beam decreases with increasing surface temperature. These trends are in agreement with a model proposed by Beeby,[26] who proposed that the variation of the specular intensity with the above mentioned factors could be explained by a Debye–Waller factor. The model predicts that

$$I/I_0 = \exp - \left[\frac{48 m_g E_i T}{2 m_s k (\theta_D^s)^2} (\omega^2 \cos^2 \theta_i + D/E_i) \right], \qquad (1)$$

where I is the specular intensity, I_0 is the incident beam intensity, m_g is the mass of the incoming particle, m_s is the mass of a surface atom, E_i and θ_i are the beam energy and angle of incidence, respectively, D is the attractive well depth, θ_s^D is the surface Debye temperature, k is the Bolzmann constant, and T is the substrate temperature.

Figure 3 shows the variation of I/I_0 with substrate temperature. The experimental data are in qualitative agreement with the predicted exponential variation with temperature. An extrapolation to $T=0$ yields $I/I_0=1$, showing that the surface is largely defect free and indicates that, even at very low temperatures, additional diffraction beams if present will have very low intensity. The model permits an evaluation of θ_s^D from the data in Fig. 3 since all quantities except D in Eq. (1) are known. The value obtained for θ_s^D is 333 K for $D=0$ and 386 K for $D=250$ cal/mole. Both values are higher than the bulk Debye temperature θ_B^D of 270 K, whereas it is expected that $\theta_B^D \sim 1.5\,\theta_s^D$.[27] Other experiments on metal surfaces[28,29] have shown that θ_s^D obtained from Eq. (1) is always higher than θ_B^D. The model proposed[26] is inadequate for incoming particles whose veloc-

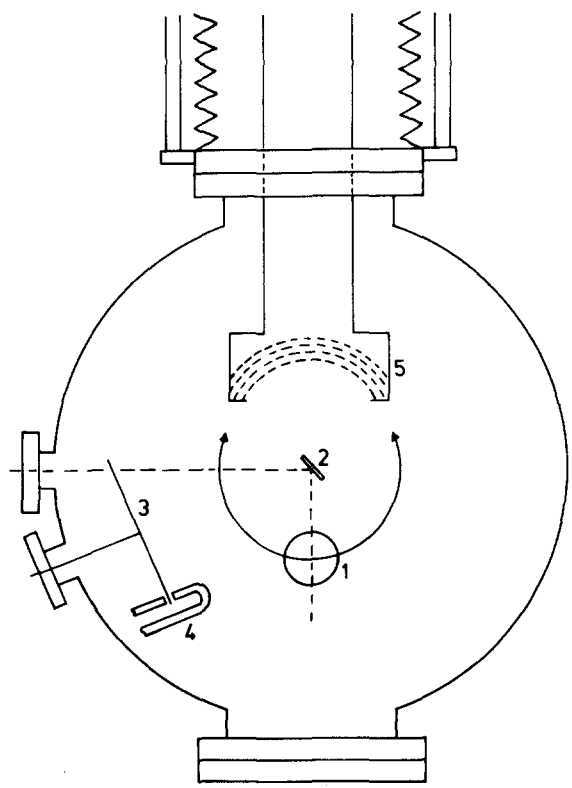

FIG. 2. Schematic diagram of the UHV apparatus. The quadrupole can be rotated about the crystal in the scattering plane: 1, quadrupole mass spectrometer, 2, Pd (111) crystal, 3, chopper, 4, lightpipe,, 5, LEED–AES analyzer.

ities are thermal and which, through the long range attractive potential, feel the coordinated motion of several surface atoms during the interaction time of a scattering event.[27]

Adsorption of gases on single crystal metal surfaces has generally been reported to decrease the specular He intensity.[1] Figure 4 shows the decrease in I/I_0 as a function of CO coverage. (The assignment of CO coverages will be discussed in Sec. III.B). It is seen that the intensity decreases more rapidly than the increase in coverage and that for $\theta = 0.1$, I/I_0 has decreased to half its initial value. For large CO coverages, I/I_0 decreases to a value consistent with a cosine distribution in all planes normal to the surface.

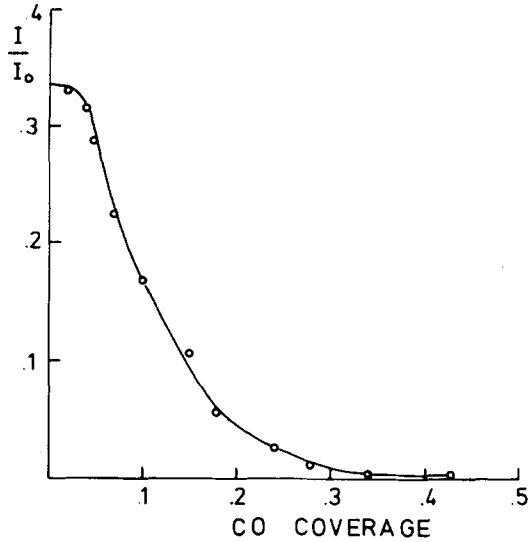

FIG. 4. Normalized He specular intensity I/I_0 as a function of the CO coverage θ. Angle of incidence = 45°.

B. Scattering of CO from Pd(111)

Figure 5 shows the angular distribution of CO scattered from a Pd(111) surface for two different substrate temperatures. The measurements have been carried out under equilibrium conditions so that the coverages are the saturation values at the indicated temperatures and at a beam intensity which corresponds to an effective pressure of $\sim 4 \times 10^{-7}$ torr (see below). The saturation coverages at 300 and 1020 K are $\theta = 0.5$ and $\theta = 10^{-7}$, respectively. The following conclusions may be drawn from these measurements:

(i) The angular distribution of scattered CO is nearly cosine with a very small lobular contribution centered near the specular angle.

(ii) The angular distribution of scattered CO is coverage independent for $\theta < 0.5$.

(iii) The angular distribution of scattered CO is independent of substrate temperature between 300 and 1200 K.

(iv) The values of I/I_0 obtained for CO scattering are consistent with a cosine distribution in all planes normal to the surface.

Since the angular distribution is independent of coverage, the absolute sticking coefficient S can be determined at a single detector position by observing the scattered signal I as a function of time and S is given by

$$S(t) = 1 - I(t)/I(\infty), \tag{2}$$

where S is an implicit function of θ through t.

Figure 6 shows a plot of I vs t. An absolute determination of the initial sticking coefficient S_0 can be made without knowledge of the beam intensity using Eq. (2). In order to determine $S(\theta)$ the beam intensity must be known.

A calibration was made by comparing the area under flash desorption curves obtained by adsorbing from the beam and from an isotropic CO pressure in the system.

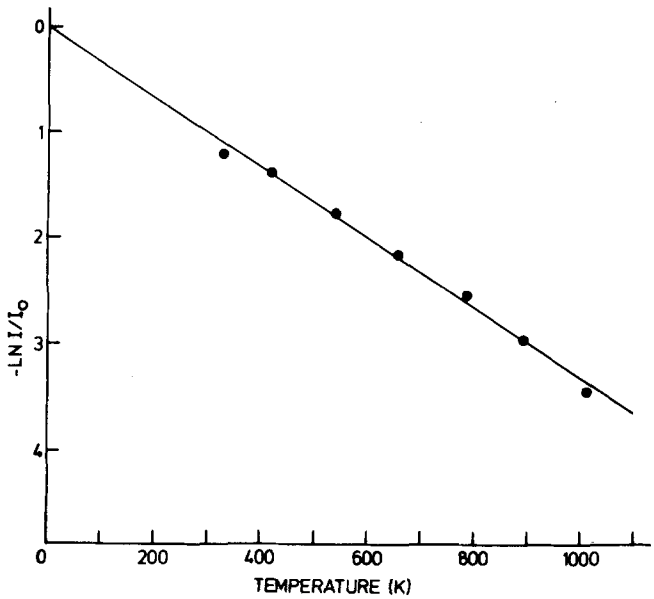

FIG. 3. Natural logarithm of the specular He intensity I normalized to the incoming beam intensity I_0 as a function of temperature. Angle of incidence = 45°.

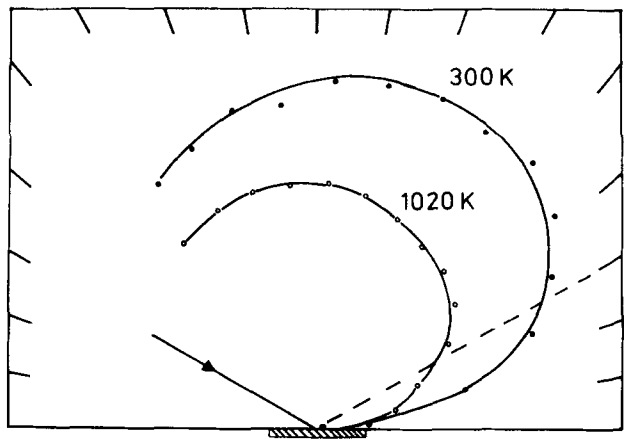

FIG. 5. Angular scattering distribution in the scattering plane for CO scattered from Pd (111) for substrate temperatures of 300 and 1020 K. Angle of incidence = 60°.

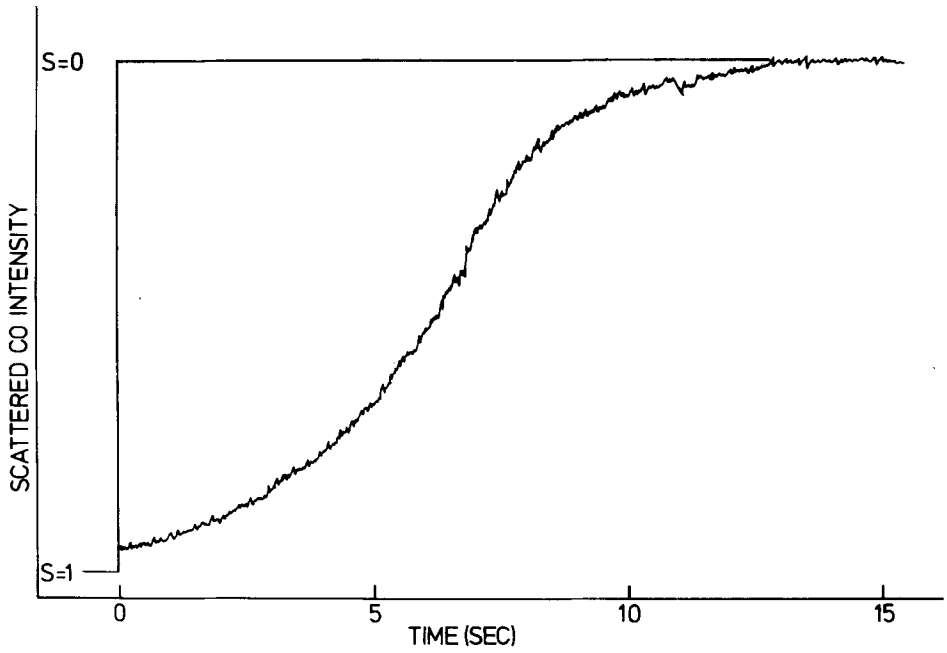

FIG. 6. Scattered CO intensity as a function of time for an initially clean Pd (111) surface. The vertical distance between the curve and the horizontal asymptote for long times gives the absolute sticking coefficient. The circumscribed area is proportional to the coverage.

It was verified that the contribution from the back side of the crystal to the area under the peak was negligible for adsorption from the isotropic CO pressure. The maximum CO beam intensity obtained is 1.5×10^{15} molecules/cm^2 s, which is equivalent in arrival rate to a pressure of 4×10^{-7} torr. The uncertainty in this value is estimated to be ±20%.

Using this beam calibration, $S(\theta)$ for 374 K and an effective sticking coefficient for two higher temperatures are shown in Fig. 7. The initial sticking coefficient S_0 is nearly unity and the decrease in S with θ is less than linear, indicating that $S(\theta)$ can be described by a precursor state model. The saturation coverage at 300 K is approximately $\theta=0.5$, in good agreement with previous LEED studies.[17] No dependence of S_0 on temperature is seen for $T<650$ K; for $T>650$ K the equilibrium coverage is below the detection limit. This is consistent with the data in Fig. 5, which suggest that even for scattering at 1020 K all CO molecules are initially adsorbed and subsequently desorbed. The accuracy of S_0 is estimated to be ±5%, whereas the uncertainty in $S(\theta)$ is primarily due to the assignment of θ to a value of $I(t)$ based on the beam intensity calibration.

It should be emphasized that Eq. (2) gives a sticking coefficient in the usual sense (chemisorption for a time $\tau\to\infty$) only if thermal desorption can be neglected. In general, the signal at the detector is given by

$$I=f(\Omega)\{I_0[1-S(\theta)]+\theta\nu\exp[-E_{\rm des}(\theta)/RT]\},$$

where $f(\Omega)$ is a function which describes the angular scattering distribution and ν and $E_{\rm des}(\theta)$ are the preexponential factor and activation energy for desorption, respectively. The function $f(\Omega)$ will not in general be identical for thermal desorption and for scattering without sticking. As the angular distribution in Fig. 5 shows, this is, however, the case for CO scattering from Pd(111).

The 374 K curve in Fig. 7 corresponds to negligible desorption for $\theta<0.45$. The desorption rate dn/dt for a constant temperature and for $T>374$ K at constant θ is given by

$$dn/dt=I_0[S(374)-S(T)] \tag{4}$$

directly. In addition, extrapolation of the curves to $S=0$ yields the equilibrium coverage θ_E. Since

$$I_0S(\theta_E)=\theta_E\nu\exp[-E_{\rm des}(\theta)/RT], \tag{5}$$

a rough estimate of the coverage dependence of $E_{\rm des}$ can be made by measuring θ_E at various temperatures, extracting $S(\theta_E)$ from the 374 K curve in Fig. 7, and cal-

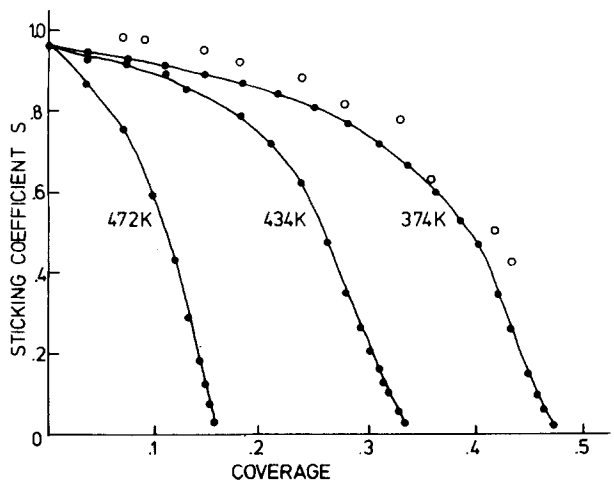

FIG. 7. Sticking coefficient S (374 K curve) and effective sticking coefficients for substrate temperatures of 434 and 472 K. (•) without beam modulation; (o) beam modulation frequency = 17 Hz.

culating $E_{des}(\theta_E)$ from Eq. (5) using the known value of I_0 and ν (see Sec. III. D). This treatment assumes that S is only a function of θ and is independent of T. Although the measurements described show only that $S_0 \neq S(T)$, modulated beam measurements described in Sec. III. D indicate that this is also true for $\theta \neq 0$. The results show that $E_{des}(\theta)$ decreases approximately linearly with θ from 32 kcal/mole at low coverages to 26 kcal/mole at $\theta = 0.42$. These values are, in view of the simplicity of the model, in reasonable agreement with isosteric heat measurements.[17]

For several adsorption systems an angular dependent sticking coefficient has been reported in the literature.[9] Measurements for CO on Pd(111) were made by integrating the area under flash desorption peaks for a fixed angle α between the incoming beam direction and the surface normal. Four different exposures were made in the initial coverage range in which S varies only slightly with coverage. A linear relationship between the area under the desorption peak and the exposure was found and the slopes of such plots at different angles α were compared. For S independent of α a linear relationship between the slope dN/dt and $\cos\alpha$ is expected. The results shown in Fig. 8 indicate that, to within the experimental error, the sticking coefficient is independent of the angle of incidence.

C. Scattering of O_2 from Pd(111)

The angular distribution of scattered O_2 was obtained by measuring a set of curves such as those shown in Fig. 6 for various scattering angles at constant incident angle. From this set an angular distribution at each coverage below the saturation value can be extracted. Figure 9 shows the results obtained for $\theta = 0$ and for saturation at 300 K, which corresponds to $\theta = 0.25$.[18] It is seen that, in contrast to CO scattering, the angular distribution is strongly coverage dependent. For both coverages a cosine component and a lobular component centered near the specular angle can be clearly distinguished. The effect of increasing the oxygen coverage is to shift intensity from the lobular to the diffuse component. The maximum intensity in the lobe is less than a factor of 2 higher than that obtained for CO at the same angle indicating appreciable out of plane scattering for the lobular component. This result is in contradiction to the predictions of the cube models[30] and in view of the highly specular He scattering cannot be attributed to surface roughness. At the surface temperatures used here, thermal desorption from the chemisorbed state is negligible.

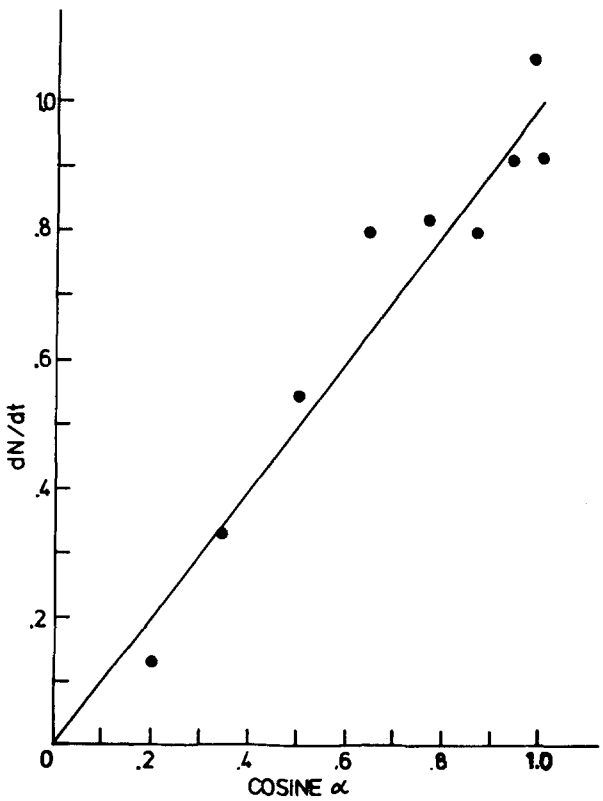

FIG. 8. CO adsorption rate dN/dt as a function of the angle of incidence α.

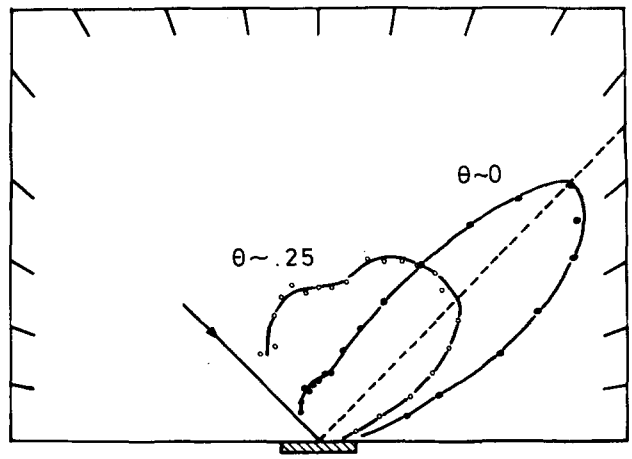

FIG. 9. Angular scattering distribution in the scattering plane for O_2 scattered from Pd (111) at 420 K for coverages of $\theta = 0$ and $\theta = 0.25$. Angle of incidence = 45°.

Since the angular scattering distribution is coverage dependent, the method described in Sec. II. B to measure S is not applicable. An alternative method has been described by King *et al.*[6] and by Madey[7] in which the scattered molecules are detected as a pressure rise in the chamber after equilibration with the chamber walls. For these measurements it is essential that the beam diameter is smaller than the crystal in order to ensure that no spurious pressure rise occurs due to beam molecules which do not strike the surface. The results are shown in Fig. 10 for two substrate temperatures. Due to the high pumping speed of the system, the signal is much smaller than for the method described in Sec. II. B. The beam intensity was not calibrated and the coverage at which S approaches zero was assumed on the basis of a LEED study[18] to be $\theta = 0.25$. It is seen that S decreases approximately linearly with coverage. The crossover of the curves for $\theta \sim 0.2$ is within the error limit and need not imply activated adsorption at high coverages. As is seen in Fig. 11, S_0 falls linearly with increasing substrate temperature for $T < 500$ K. The angular dependence of S can be measured in the same way as for CO adsorption. Data points obtained

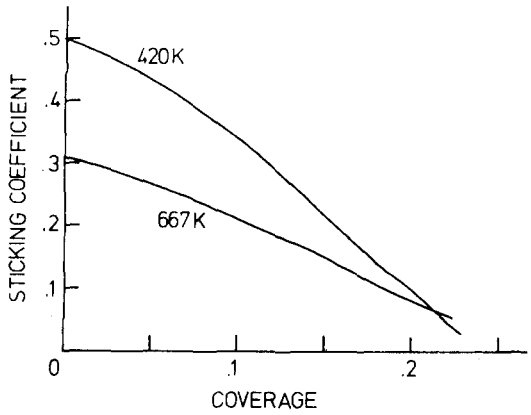

FIG. 10. Sticking coefficient S as a function of coverage for O_2 on Pd (111) for substrate temperatures of 420 and 667 K.

with both flash desorption and with AES are shown in Fig. 12. To within the experimental error, no marked deviation from the solid line which is the behavior expected for S independent of the angle of incidence α is obtained.

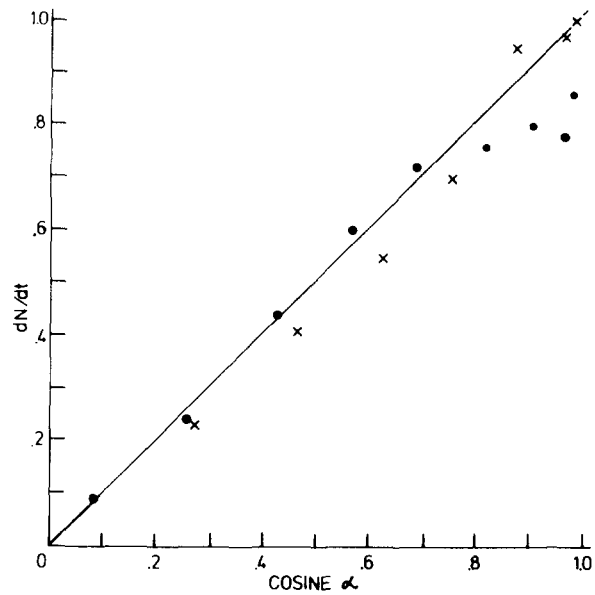

FIG. 12. O_2 adsorption rate dN/dt as a function of the angle of incidence α. (•) from flash desorption; (x) from AES.

D. The interaction of a modulated CO beam with Pd(111)

Amplitude modulation of a beam before impingement on the surface combined with phase sensitive detection allows a determination[5,31] of the relaxation time associated with the surface process. For high temperatures and low coverages, desorption is rate limiting and for first order desorption the residence time is the inverse desorption rate. The measurements were carried out by impinging the chopped beam of intensity I_0 on the surface whose temperature was varied. The surface coverage under these conditions is determined by I_0, $S(\theta)$, and the residence time τ and increases with decreasing temperature [see Eq. (7)]. The results obtained with phase sensitive detection for the amplitude J at the modulation frequency CO and the phase lag ϕ referenced to zero residence time are shown in Fig. 13 as a function of the substrate temperature. Results are shown for $\omega = 0$ and $\omega = 18$ Hz. Since the detector measures the density of the gas molecules in the ion source, the sensitivity varies inversely with molecular velocity. For complete accomodation with the surface, J for $\omega = 0$ should fall off as $T^{-1/2}$. The open circles which are calculated from $J(500) \times \sqrt{500}/T$ agree qualitatively with the data. The deviation from the predicted behavior for $T > 500$ K is probably due to slight changes in the angular distribution rather than to lack of accommodation, whereas it is possible that the deviation for $T < 500$ K may be due to incomplete accommodation since the residence time is below the detection limit ($\sim 2 \times 10^{-5}$ s). For $\omega = 18$ Hz a marked demodulation of the signal accompanied by a large phase lag is seen. A discussion of the results can be subdivided into the temperatures 500–700 and 300–500 K.

For temperatures above 500 K the dominant features are the nearly complete demodulation of J near 500 K and the large changes in J and ϕ between 550 and 650 K. Since J is nearly zero at 500 K, nearly every scattering event leads to chemisorption associated with a mean

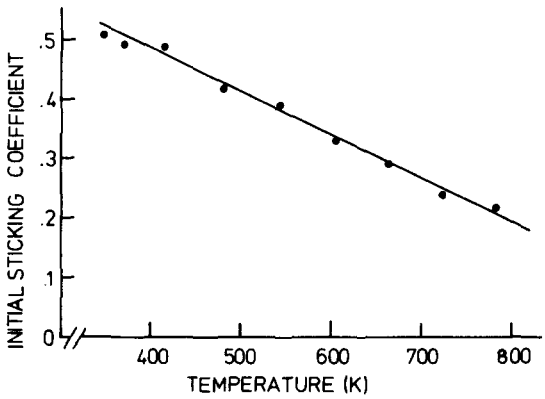

FIG. 11. Initial sticking coefficient S_0 for O_2 on Pd (111) as a function of the substrate temperature.

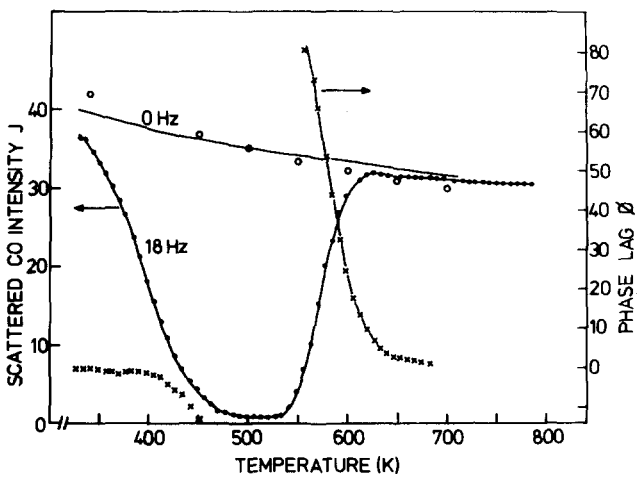

FIG. 13. Intensity J (•) and phase lag ϕ (x) as a function of substrate temperature for CO scattering with O and 18 Hz modulation.

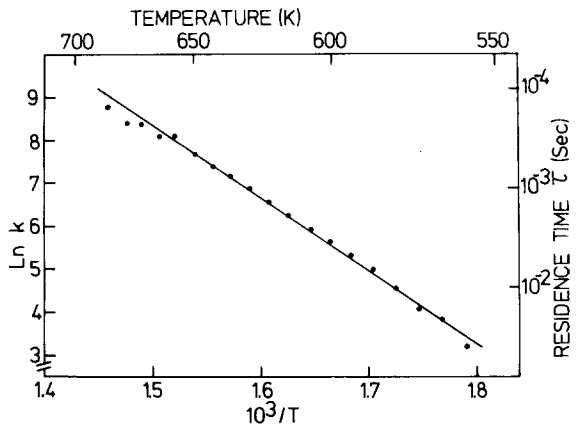

FIG. 14. Natural logarithm of the rate constant for desorption k as a function of the substrate temperature for CO scattering from Pd (111).

residence time $\tau \gg 1/\omega$. With increasing temperature τ decreases exponentially and J and ϕ change in accordance with[5]

$$J/J_0 = (1 + \omega^2\tau^2)^{-1/2} \tag{6}$$

and

$$\phi = \tan^{-1}\omega\tau ,$$

where J_0 is the amplitude for $\omega = 0$.

Since τ is given by[5]

$$\tau = \nu^{-1}\exp(E_{des}/RT) , \tag{7}$$

where E_{des} and ν are the activation energy and pre-exponential factor for desorption, respectively, the data in Fig. 13 can be used to determine E_{des} and ν. The results are shown in Fig. 14. The experimentally determined values are $E_{des} = 32 \pm 2$ kcal/mole and $\nu = 10^{14.4\pm0.8}$. The value obtained for E_{des} is in good agreement with the isoteric heat at low coverages of 34 kcal/mole[17] and ν is in the range predicted by simple models[32] of the desorption process. In the temperature range used the equilibrium coverage is less than $\theta = 0.01$ so that the method gives E_{des} and ν in the limit of zero coverage.

For temperatures below 500 K, J increases with decreasing temperature, whereas ϕ changes only slightly. This behavior is consistent with a decrease in S with increasing coverage. Those molecules which are chemisorbed are completely demodulated, whereas those which have a residence time τ such that $\omega\tau \ll 1$ are detected without significant demodulation or phase lag. $S(\theta)$ can be extracted from the measured values of

$$1 - J(18\text{ Hz}, T)/J(0\text{ Hz}, T) \tag{8}$$

and the known equilibrium coverage at the temperature T. The results are shown as the open circles in Fig. 7. The agreement with the 374 K curve is good; the slight shift to lower coverages for the unchopped curve is within the experimental error. Since each data point corresponds to a different temperature, the agreement shows that $S(\theta)$ is independent of temperature even at temperatures at which the desorption rate is large.

This method of evaluating S is equivalent to defining sticking as chemisorption with a residence time $\tau > 10^{-1}$ s since for these residence times $J/J_0 < 0.1$ at the modulation frequency used.

The results for J/J_0 and ϕ for $T < 500$ K are consistent with a saturation of the surface sites at 300 K at which the activation energy for desorption is more than 12 kcal/mole ($\tau \sim 10^{-4}$ s). This is also in agreement with the observation that, whereas an increase in ω shifts the high temperature region of rapidly changing ϕ and J/J_0 to higher temperatures, the low temperature region is unaffected by changes in the modulation frequency.

The negative phase lag which is observed below 500 K suggests that more information can be obtained through direct observation of the scattered CO waveform. The data obtained with a digital signal averager is shown in Fig. 15. For substrate temperature of 330 and 784 K the residence time is so short that no waveform distortion is observed. The distortion observed in the 559 and 583 K curves is that expected[33] for first order desorption and $\omega\tau \sim 1$. However, the waveforms for 522 and 472 K show unexpected features, such as the transients observed when the beam is switched on and off and the antiphase relationship between the incoming and the scattered beam, which was seen as a negative phase shift with phase sensitive detection. These effects can be seen more clearly for slight surface carbon contamination since J/J_0 is larger, allowing reliable determinations of ϕ. The waveform is shown in Fig. 16. The 532 K waveform is similar in shape to the incoming waveform but corresponds to a phase lag of more than 200°. For 433 and 484 K the waveforms

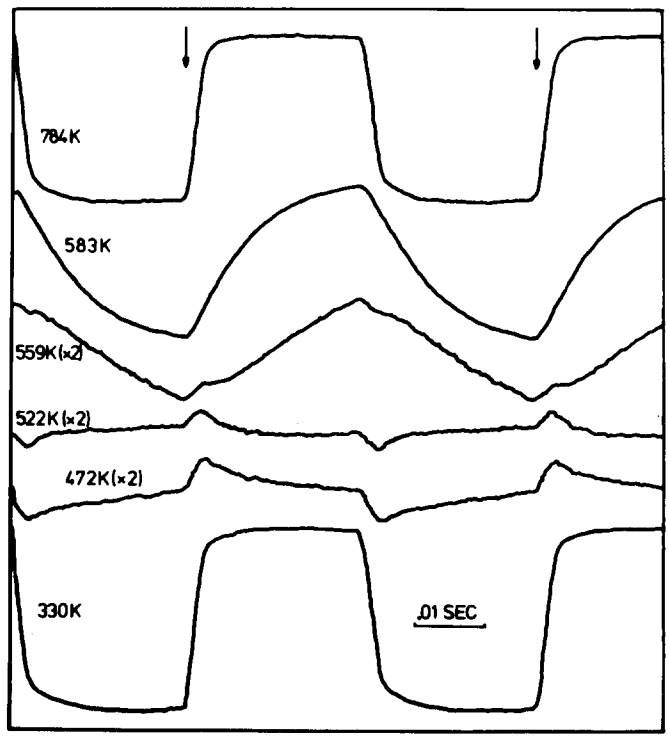

FIG. 15. Digitally averaged waveforms for CO scattered from Pd (111). The arrows indicate the times at which the beam is switched on. Modulation frequency = 18 Hz.

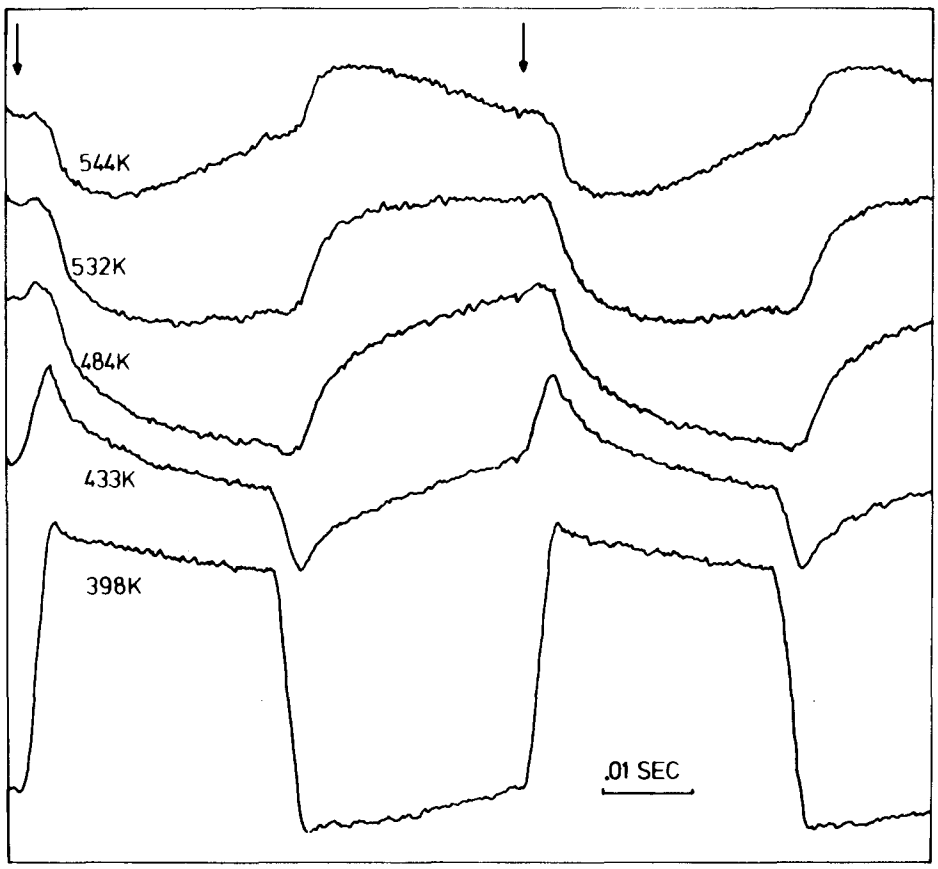

FIG. 16. Digitally averaged waveforms for CO scattered from a Pd (111) surface contaminated with carbon. The arrows indicate the times at which the beam is switched on. Modulation frequency = 18 Hz.

show more clearly the features seen somewhat indistinctly in Fig. 15. The sharp transients are seen best at 433 K. Further cooling to 398 K leads to a mixture of the waveforms with transients and the undistorted waveform; the addition of the transients sharpen up the leading and trailing edges. The form of all of these curves for $T < 520$ K can basically be seen as a superposition of waveforms like that observed at 532 K (Fig. 16) and the undistorted waveform; since ϕ for the 532 K waveform is greater than 180°, the superposition gives rise to sharp symmetrical features which are positive at the beginning and negative at the end of the waveform. This superposition with the undistorted waveform becoming predominant at low temperatures is consistent with a decrease in S for $T < 530$ K due to the increasing surface coverage. The corresponding data for the carbon contaminated surface obtained with phase sensitive detection is shown in Fig. 17. The falloff in $S(\theta)$ with increasing coverage has been corrected for by assuming that $S(\theta)$ is unchanged by the contamination. It is seen that ϕ increases rapidly to approximately 180° as the temperature decreases before asymptotically approaching a value of 210°. J/J_0 falls off more slowly than for the clean surface for $T < 600$ K. This allows a detailed waveform analysis at low temperatures which was not possible for the clean surface.

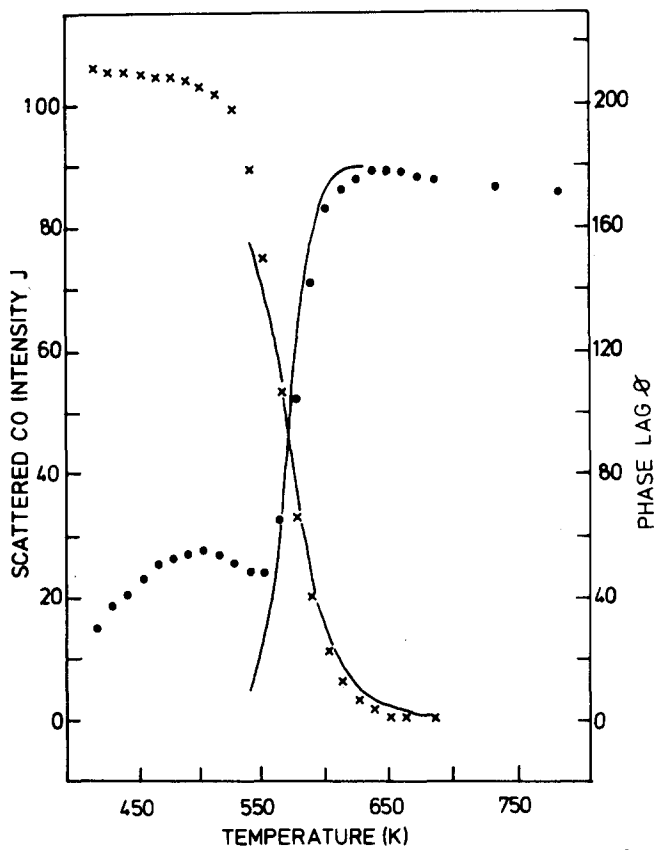

FIG. 17. Intensity J (•) and phase lag ϕ (x) as a function of substrate temperature for a carbon contaminated surface. Modulation frequency = 18 Hz. The solid lines give the curves calculated from Eq. (21) with $k_b = k_c = 5 \times 10^{13} \exp(-31\,000/RT)$.

E. Thermal desorption of CO and O_2 from Pd(111)

The angular distribution for thermal desorption of CO from Pd(111) was measured by recording the angular distribution for a scattered CO beam at a substrate tem-

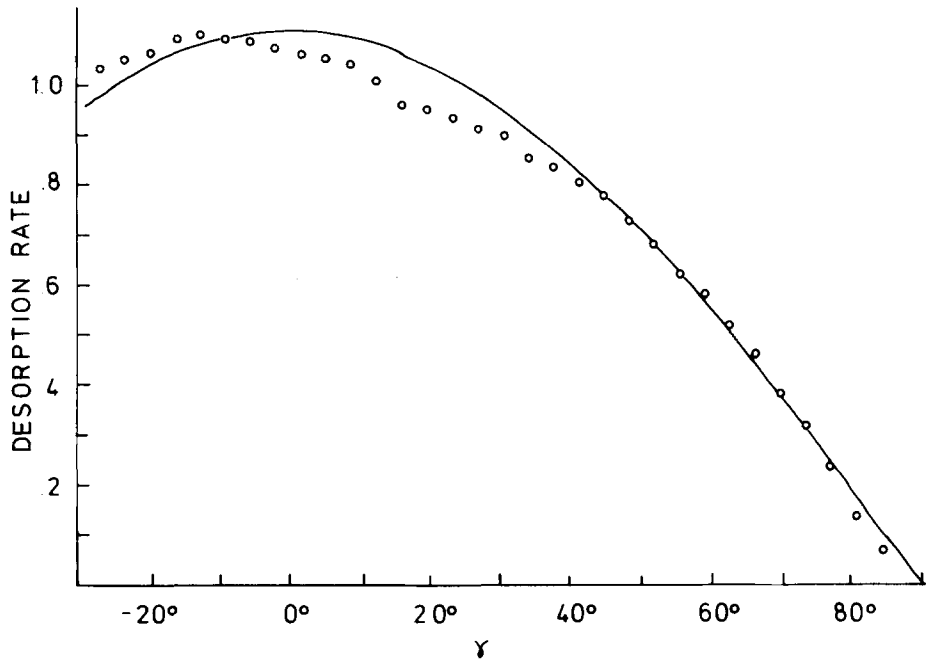

FIG. 18. Angular distribution in the scattering plane for CO desorption at 500 K. The angle is measured from the normal to the surface. (o) data points. The solid line is the result expected for a cosine distribution. Angle of incidence = 50°.

perature of 500 K. From Figs. 13 and 14 it can be seen that at this temperature the residence time is greater than 10^{-2} s and that nearly all ($J/J_0 < 0.04$) of the CO molecules have such long residence times that one can therefore be sure that the angular distribution corresponds to thermal desorption from a chemisorbed layer. The results are shown in Fig. 18. No marked deviation from a cosine distribution is seen.

For O_2 the angular distribution in the temperature range at which desorption occurs (800–1100 K) is a mixture of lobular and cosine scattering since $S < 0.3$. The angular distribution for desorption was therefore measured by the flash desorption technique. After adsorption of O_2 to $\theta = 0.1$, the crystal was oriented at a fixed angle to the quadrupole and then flashed. Since the system has a high pumping speed for O_2, the correction due to the pressure rise in the system was small and could easily be made. The results are shown in Fig. 19. A slight forward peaking of the distribution is seen; however, the deviation from a cosine function is not appreciable. In view of the integral information obtained with the flash desorption technique, a more detailed analysis of the results is not justified.

Recent studies[34,35] have emphasized that a cosine distribution with a Maxwellian velocity distribution characteristic of the substrate temperature may be the exception rather than the rule. Application of the principle of detailed balancing[35] predicts that an angular dependence of the sticking coefficient should be observed if the desorption is noncosine and non-Maxwellian. Neither of these effects is seen for O_2 and CO on Pd(111). This may be due to the strong interaction between the adsorbate and the surface and the use of beams at thermal energies and need not necessarily be true at all beam energies.

IV. DISCUSSION

A. Helium scattering from clean and adsorbate covered Pd(111)

The results discussed in Sec. IV.A show that although the crystalline order for the clean surface is good, no meaningful surface Debye temperature can be extracted from the model. For an adsorbate covered surface it has previously been reported that the specular intensity falls with increasing coverage[1] and that diffuse scattering is either directly observed or is inferred from the values of I/I_0. The mechanism which has been proposed to explain this phenomena is that the scattering particle effectively sees a surface of lower mass and that the possible energy and momentum transfer is enhanced.[36] Recent measurements indicate that an alternative explanation may be applicable. Helium is scattered diffusely from a polycrystalline oxygen covered tungsten surface although a velocity analysis of the

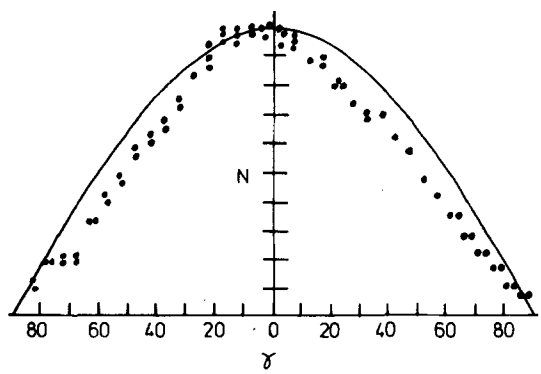

FIG. 19. Angular distribution for thermal desorption O_2. (•) data points. The solid line is the result expected for a cosine distribution.

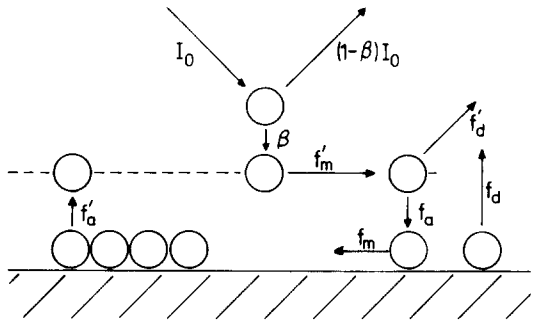

FIG. 20. Schematic diagrams of the possible scattering channels for adsorption and desorption involving a precursor state. β is the probability for capture in the precursor state which is represented by the dashed line. f'_m, f'_d, and f'_a are the probabilities for diffusion, desorption, and adsorption for the precursor state, respectively. f_m and f_d are the probabilities for diffusion and desorption for the chemisorbed state, respectively. f_a is the probability of activation from the chemisorbed to the precursor state.

scattered atoms shows that little accomodation has taken place.[37] It has also been observed[38] that He scattering from a $p(2\times1)$ oxygen structure on W(110) gives rise to strong diffraction features although no diffraction was seen for the clean surface. Both observations are consistent with an increased corrugation of the potential at the surface upon adsorption; for an ordered array of O adatoms diffraction is observed, whereas scattering from the disordered array on the polycrystalline surface gives rise to a diffuse scattering distribution:

This suggests that the decrease in I/I_0 with CO coverage shown in Fig. 4 may be due to the disorder in the adlayer rather than to accommodation. This is in agreement with the observation that the additional LEED spots, although clearly visible, are not sharp for either CO or O_2 adsorption at 300 K. The greater sensitivity of the scattering for disorder—although the coherence length are similar to those for LEED—is due to the difference in the details of the interaction. At the electron energies typical for LEED the scattering is predominantly from the core potentials and three to four atom layers contribute to the scattering. For thermal atom and molecular beams, scattering is due mainly to the repulsive interaction between the valence electron distributions in the substrate and beam particle and only one layer contributes to the scattering. Slight displacement of adatoms can influence the valence electron distribution significantly, without greatly changing the periodic array of the core potentials and may lead to different sensitivities for surface disorder for the two methods. Disorder may also be responsible for the largely diffuse angular distributions shown in Figs. 5 and 9. In both cases the residence time is less than the detection limit and the diffuse nature of the distribution may be due to scattering from an effectively rough surface rather than being indicative for energy accommodation. This possibility must be taken into account when interpreting the angular distributions in connection with the adsorption–desorption process.

B. Adsorption kinetics of O_2 and CO on Pd(111)

The processes which can occur when a molecule impinges on a surface have been described previously[39,40] and are shown schematically in Fig. 20. The initial scattering can lead to capture in a precursor state with a probability β or to scattering back into the gas phase with a probability $1-\beta$ and an angular distribution $f_{1-\beta}(\Omega)$. The fraction β of the molecules are initially captured in the precursor state for a mean residence time τ, after which they are either desorbed with probability f'_d and angular distribution $f_\beta(\Omega)$, diffuse over the surface with probability f'_m, or are chemisorbed at an empty site with probability f_a. For temperatures at which thermal desorption from the chemisorbed state is negligible, the total backscattered intensity is the sum of the directly backscattered intensity and the desorption from the precursor state. A distinction between these two scattering channels which together are the first term in Eq. (3) is only possible on the basis of their differing angular distributions since time of flight techniques cannot resolve the $\sim10^{-13}$ s interaction time for direct scattering and the $\sim10^{-9}$ s residence time for a precursor molecule at 300 K (assuming $E_{des}=3$ kcal/mole and $\nu=10^{13}$ s^{-1} in the precursor state). Since by definition the directly backscattered molecules have a vanishingly small residence time on the surface, their angular distribution $f_{1-\beta}(\Omega)$ should be similar to that observed for the scattering of rare gases of comparable masses. This is clearly the origin of the lobular scattering of O_2 at low coverages shown in Fig. 9. The observed half width of 37° for the lobe at $\theta=0$ agrees well with the value of 38° which has been reported[41] for Ar scattering from Ag(111) at equivalent beam energies. Molecules which are desorbed from the precursor state have a sufficiently long surface residence time for thermal accommodation so that in a first approximation, $f_\beta(\Omega)$ should be a cosine function. This is the origin of the diffuse scattering for O_2 at low coverages and for the diffuse CO scattering with residence times below the detection limit when $\theta>0.1$. Since $\beta\geq S$, β for CO at low coverages is essentially unity. Using the initial sticking coefficient for O_2 from Fig. 11 of 0.4 and estimating the contribution of the diffuse component at low coverages in Fig. 9 to be 10% of the total backscattered intensity, β for O_2 is estimated to be 0.5 at 520 K. At higher coverages τ is small and the effect of surface roughening discussed in Sec. IV.A cannot be neglected for either O_2 or CO adsorption. Although both scattering channels for O_2 adsorption are clearly seen at $\theta=0.25$, no separation into $f_\beta(\Omega)$ and $f_{1-\beta}(\Omega)$ is possible since the increased surface roughening makes $f_{1-\beta}(\Omega)$ coverage dependent. Since no change in the angular distribution for CO scattering is observed at high temperatures, it can be concluded that β is constant at roughly unity independent of surface temperature. For O_2 adsorption the intensity at the specular angle is unchanged with increasing surface temperature, showing that the temperature dependence on S_0 shown in Fig. 11 is dominated by the probabilities of the surface properties in Fig. 20 and not by a decrease in β.

The form of $S(\theta)$ depends on the relative probabilities of the processes shown in Fig. 20. $S(\theta)$ for both CO and O_2 adsorption can be reasonably well described by the Kisliuk model and its modifications.[42-44] The models however assume that the probabilities of all the processes shown in Fig. 20 are independent of coverage, which is a major simplification. Further simplifications are made in the temperature dependence of S_0 in which the substrate appears only implicitly through the activation energies for adsorption, desorption, and diffusion. Similarly, the models cannot explain the linear decrease in S_0 with temperature for O_2 adsorption.

C. CO scattering from Pd(111) using modulation techniques

Since the probability β of a CO molecule being captured in the precursor state is unity, a scattering event always involves initial capture. The CO molecule can desorb from the precursor state or be chemisorbed. Since the lifetime τ of a molecule in the precursor state is only of the order of 10^{-9} s at 300 K, sticking as discussed in Sec. III.B is associated only with chemisorption and not with capture in the precursor state. Subsequent desorption of the CO molecule from the chemisorbed state can also take place.

The possible processes can be expressed by the following kinetic model:

$$\begin{array}{ccccc} CO_g & - & CO_p & \underset{k_3}{\overset{k_2}{\rightleftarrows}} & CO_{ad} \xrightarrow{k_4} CO_g \\ & & \downarrow k_1 & & \\ & & CO_g & & \end{array} , \tag{9}$$

in which CO_p and CO_{ad} denote a molecule in the precursor state and the chemisorbed state, respectively, and $k_1 - k_4$ are rate constants associated with the transitions indicated. These constants may not be independent of coverage. In particular, k_1 is an effective rate constant which increases with increasing coverage since, for saturation of the chemisorption layer, all molecules will be scattered directly from the precursor state back into the gas phase. The kinetic equations for the above model are given by

$$\begin{aligned} \frac{dCO_p}{dt} &= -(k_1+k_2)CO_p + k_3 CO_{ad} + I_0 \beta g(t) , \\ \frac{dCO_{ad}}{dt} &= k_2 CO_p - (k_3+k_4)CO_{ad} , \\ \frac{dCO_g}{dt} &= k_4 CO_{ad} + k_1 CO_p , \end{aligned} \tag{10}$$

where $g(t)$ is the chopper gating function and β is the capture probability in the precursor state.

The amplitude and phase lag ϕ of the scattered CO signal for the above model can be calculated using the method of Chang and Weinberg.[31] In their nomenclature the matrices K, Q, and Q^{-1} and the eigenvalues of K are given by

$$K = \begin{pmatrix} -[k_1+k_2] & k_3 \\ k_2 & -[k_3+k_4] \end{pmatrix} , \tag{11}$$

$$Q = \begin{pmatrix} \dfrac{\lambda_- + k_3 + k_4}{k_2} & \dfrac{\lambda_+ + k_3 + k_4}{k_2} \\ 1 & 1 \end{pmatrix} , \tag{12}$$

$$Q^{-1} = \frac{k_2}{\lambda_- - \lambda_+} \begin{pmatrix} 1 & -\dfrac{(\lambda_+ + k_3 + k_4)}{k_2} \\ -1 & \dfrac{(\lambda_- + k_3 + k_4)}{k_2} \end{pmatrix} , \tag{13}$$

and

$$\lambda = \frac{-(k_1+k_2+k_3+k_4) \pm \sqrt{(k_1+k_2)^2 + (k_3+k_4)^2 + 2k_2k_3 - 2k_1(k_3+k_4) - 2k_2k_4}}{2} . \tag{14}$$

The phase lag ϕ is calculated to be

$$\tan\phi = \frac{\omega[k_2k_4(k_1+k_2+k_3+k_4) + k_1k_3(k_2+k_3+2k_4) + k_1(k_4^2+\omega^2)]}{\omega^2[k_1^2 + k_2(k_1-k_4)] + (k_1k_3 + k_1k_4 + k_2k_4)^2} . \tag{15}$$

Since all terms in the numerator are positive, whereas the denominator can be either positive or negative depending on the relative magnitudes of the rate constants ϕ at a given temperature lies between 0° and 180°. For $k_1 > k_4$, $90 > \phi > 0$, and for $k_1 < k_4$, ϕ can assume values up to 180°. Due to the complexity of the above expression, the temperature dependence of ϕ can in general only be evaluated numerically for assumed values of the rate constants. However, two special cases of the kinetic model in Eq. (9) lead to a simpler expression.

1. CO scattering from a saturated chemisorbed layer

For this case $k_1 \gg k_2$, k_3, $k_4 \approx 0$ and $\tan\phi = \omega/k_1$. Since $k_1 \gg \omega$, $\phi \approx 0$ and $J/J_0 \approx 1$. This behavior is very nearly realized for CO scattering at 300 K.

2. CO scattering for substrate temperatures $T > 500$ K

As is shown in Fig. 13, J/J_0 is nearly zero near 500 K. This shows that backscattering from the precursor state directly into the gas phase is negligible at low coverages and implies that $k_2 \gg k_1$. Desorption of CO can proceed either directly over the reaction path corresponding to rate constant k_4 or via the precursor state over the path corresponding to the rate constants k_3 and k_1. For direct desorption the kinetic model in Eq. (9) with $k_1 = 0$ applies. This leads to a predicted phase lag

$$\tan\phi = \frac{\omega(k_2+k_3+k_4)}{k_2k_4 - \omega^2} , \tag{16}$$

which, for k_2, $k_4 \gg k_3$, leads to the result for a series process[5,31]

$$\phi = \arctan \omega/k_2 + \arctan \omega/k_4 . \quad (17)$$

Since the activation energy associated with k_4 is E_{des} = 32 kcal/mole, whereas the activation energy associated with k_2 is of the order 5 kcal/mole, $k_2 \gg k_4$ and

$$\tan\phi = \omega/k_4 . \quad (18)$$

Since J/J_0 is nearly zero near 500 K, $k_2 \gg k_1$ and desorption from the chemisorbed layer via the precursor state can be ruled out for $T > 500$ K. Below 400 K this channel may be of importance, but since $\omega\tau \gg 1$, where τ is the residence time for a chemisorbed molecule in this range, only those molecules scattered directly back from the precursor state into the gas phase are detected. The role of the precursor in thermal desorption at high coverages has been discussed elsewhere.[45]

As is shown in Fig. 14, the kinetic model of Eq. (9) gives good agreement with the experimental results for $T > 500$ K. However, for lower temperatures and higher coverages $k_1 > k_4$ and ϕ evaluated from Eq. (15) will be less than 90°. The model is therefore not able to explain the component in the scattered waveform which has a phase lag $\phi > 180°$. As was shown in Sec. III. D, this component leads to the negative phase shifts shown in Fig. 13, which are observed for $T > 450$ K. Similarly, the model cannot predict the observed phase shifts shown in Fig. 17 for scattering from the carbon contaminated surface. Although, in principle, Eq. (17) predicts phase shifts of up to 180°, this required that $k_2 \approx k_4$ which is physically unreasonable.

For the carbon contaminated surface the kinetic model must be modified to include a further surface species since phase shifts greater than 180° require that at least three distinct types of CO be present on the surface.[5,31] A model of the type

$$CO_g \rightleftarrows CO_p \overset{k_a}{\rightleftarrows} CO(1) \overset{k_b}{\rightleftarrows} CO(2) \overset{k_c}{\rightleftarrows} CO_g \quad (19)$$

is the simplest model consistent with the results. CO(1) and CO(2) denote two species which differ either in the nature of the site at which they are adsorbed or in their internal excitations. No model in which CO dissociates or disproportionates has been considered since UPS measurements[16] show no evidence to support dissociation. The above model gives phase shifts

$$\phi = \arctan \frac{\omega}{k_a} + \arctan \frac{\omega}{k_b} + \arctan \frac{\omega}{k_c} , \quad (20)$$

which at high temperatures when $k_a > k_b, k_c$ reduces to

$$\phi = \arctan \frac{\omega}{k_b} + \arctan \frac{\omega}{k_c} . \quad (21)$$

A good fit to the data in Fig. 17 for $T > 560$ K is obtained as is shown by the dashed line for $k_b = k_c = 5 \times 10^{13} \exp(-31\,000/RT)$. It is not possible to fit the data with Eq. (21) if the activation energies of k_b or k_c differ by more than 2 kcal/mole from the above value. This implies that conversion of CO(1) to CO(2) requires an activation energy nearly equal to that for desorption. Since the carbon contaminated surface is not well defined and measurement of J/J_0 and ϕ over a wide range of frequencies ω was not possible, a more detailed kinetic model is not justified. However, a few speculations with respect to the nature of CO(1) and CO(2) can be made. It seems unlikely that the states correspond to different bonding sites, since surface diffusion with $k_b \approx 10^8 \exp(-15\,000/RT)$ should lead to interconversion. A rate constant of this form is however incompatible with the experimental results. If CO(1) and CO(2) differ by internal excitations of the CO molecule, the following model can be suggested: CO(1) desorbs preferentially via a precursor type state. However, de-excitation from the precursor type state to CO(2) occcurs with a high probability relative to the probability for desorption. For CO(2), desorption occurs directly or also via a precursor type state. For this model k_b and k_c would have nearly the same form since the activation energies would be nearly equal.

The negative phase shifts observed for the clean surface for $T < 450$ K show that a model with three surface species is also required for scattering from the impurity free surface. Since temperatures $T < 450$ K correspond to CO coverages of $\theta > 0.1$ and the carbon impurity concentration for the contaminated surface is estimated to lie in this range, it is possible that the kinetic model of Eq. (19) applies whenever the scattering CO can interact with either adsorbed CO or C, which must be present in high enough coverages to make the interaction likely. Further investigations with spectroscopic techniques would be useful to allow a more detailed understanding of these results.

V. SUMMARY

The adsorption of CO and O_2 has been studied by measuring absolute sticking coefficients and their dependence on coverage, angle of incidence, and substrate temperature. Angular scattering distributions of backscattered CO and O_2 allow one to distinguish three cases: backscattering without capture in the precursor state, scattering from the precursor state into the gas phase, and desorption from the chemisorbed state. For CO, β and S_0 are nearly unity at low coverages and are independent of the substrate temperature. For O_2, β is 0.5 at low coverages independent of the substrate temperature and S_0 falls linearly with temperature. The angular distribution for the desorption of CO and O_2 is very nearly cosine. Desorption of CO at low coverages from an impurity free surface can be analyzed in terms of simple first order desorption. The results at high CO coverages on the impurity free surface and for all CO coverages on the carbon contaminated surface can only be explained in terms of a model with three distinct adsorbed species.

ACKNOWLEDGMENTS

It is a pleasure to acknowledge valuable discussions with G. Ertl, J. Küppers, and H. Conrad throughout the course of this work and the experimental assistance of W. Becker in the initial stage of the study. Financial support by the Deutsche Forschungsgemeinschaft through Sonderforschungsbereich 128 is also acknowledged.

[1] J. P. Toennies, Appl. Phys. 3, 91 (1974).
[2] R. P. Merrill, Catal. Rev. 4, 115 (1970).

[3]H. Saltsburg, Ann. Rev. Phys. Chem. **24**, 493 (1973).
[4]W. H. Weinberg, Adv. Colliod. Interface Sci. **4**, 301 (1975).
[5]R. H. Jones, D. R. Olander, W. J. Siekhaus, and J. A. Schwarz, J. Vac. Sci. Technol. **9**, 1429 (1972).
[6]D. A. King and M. G. Wells, Surf. Sci. **29**, 454 (1972).
[7]T. E. Madey, Surf. Sci. **33**, 355 (1972).
[8]C. Kohrt and R. Gomer, Surf. Sci. **40**, 71 (1973).
[9]Ch. Steinbruchel and L. D. Schmidt, Phys. Rev. B **10**, 4209 (1974).
[10]R. Chapell and D. O. Hayward in *Adsorption-Desorption Phenomena*, edited by F. Ricca (Academic, New York, 1972).
[11]L. A. West and G. A. Somorjai, J. Chem. Phys. **57**, 5143 (1972).
[12]R. J. Madix, J. Vac. Sci. Technol. **13**, 253 (1976).
[13]J. B. Hudson and C. M. Lo, Surf. Sci. **36**, 141 (1973).
[14]M. D. Scheer, R. Klein and J. D. McKinley, Surf. Sci. **30**, 251 (1972).
[15]T. Engel and G. Ertl (to be published).
[16]H. Conrad, Thesis, Universität München, 1976 H. Conrad, G. Ertl, and J. Küppers (to be published).
[17]H. Conrad, G. Ertl, J. Koch, and E. E. Latta, Surf. Sci. **43**, 462 (1974).
[18]H. Conrad, G. Ertl, J. Koch, and E. E. Latta, Surf. Sci. **65**, 245 (1977).
[19]T. Schober, V. Sorajic, and A. Meisenberg, Metallography **8**, 359 (1975).
[20]H. Saltsburg and J. N. Smith, Jr., J. Chem. Phys. **45**, 217[illegible] (1966).
[21]S. Yamamoto and R. E. Stickney, J. Chem. Phys. **53**, 1594 (1970).
[22]G. Boato, P. Cantini, and R. Tatarek, J. Phys. F **6**, L 237 (1976).
[23]J. M. Horne and D. R. Miller, Surf. Sci. **66**, 365 (1977).
[24]D. L. Smith and R. P. Merrill, J. Chem. Phys. **52**, 5861 (1970).
[25]J. N. Smith, Jr., Surf. Sci. **34**, 613 (1973).
[26]J. L. Beeby, J. Phys. C **4**, L 359 (1971); H. Hoinkes, H. Nahr and H. Wilsch, Surf. Sci. **33**, 516 (1972).
[27]F. O. Goodman, Surf. Sci. **65**, 37 (1977).
[28]J. Lapujoulade and Y. Lejay, J. Chem. Phys. **63**, 1389 (1975).
[29]A. G. Stoll, Jr., J.-J. Ehrhardt, and R. P. Merrill, J. Chem. Phys. **64**, 34 (1976).
[30]R. N. Logan and J. C. Keck, J. Chem. Phys. **49**, 860 (1968).
[31]H. C. Chang and W. H. Weinberg, J. Chem. Phys. **66**, 4172 (1977); Surf. Sci. **65**, 394 (1977).
[32]S. Glasstone, K. J. Laidler, and H. Eyring, *The Theory of Rate Processes* (McGraw-Hill, New York, 1941).
[33]J. Perel *et al.*, J. Appl. Phys. **36**, 2157 (1965).
[34]G. Comsa, R. David, and K. D. Rendulic, Phys. Rev. Lett. **38**, 775 (1977).
[35]M. J. Cardillo, M. Balooch, and R. E. Stickney, Surf. Sci. **50**, 263 (1975).
[36]F. O. Goodman and H. Y. Wachmann, *Dynamic of Gas–Surface Scattering* (Academic, New York, 1976).
[37]D. Auerbach, C. Becker, J. Cowin, and L. Wharton, Proceedings of the VI International Symposium on Molecular Beams, Noordwijkerhout, Netherlands (1977).
[38]D. O. Hayward, R. Hodges, and K. Senkiw, in the Rideal Conference on Chemisorption and Catalysis, London (April 1977).
[39]P. A. Redhead, J. P. Hobson, and E. V. Kornelsen, *The Physical Basic of Ultrahighvacuum* (Chapman and Hall, London, 1968).
[40]F. O. Goodman, Surf. Sci. **26**, 327 (1971).
[41]H. Saltsburg and J. N. Smith, Jr., J. Chem. Phys. **45**, 2175 (1966).
[42]P. J. Kisliuk, J. Chem. Phys. Solids **3**, 95 (1957); **5**, 78 (1958).
[43]C. Kohrt and R. Gomer, J. Chem. Phys. **52**, 3283 (1970).
[44]D. A. King and M. G. Wells, Proc. R. Soc. (London) Ser. A **339**, 245 (1974).
[45]D. A. King, Surf. Sci. **64**, 43 (1977).